Profilometry-Based Indentation Plastometry Testing for Characterization of Case-Hardened Steels

Steve Ooi, Rebecca Reiff-Musgrove, Marcus Gaiser-Porter, Matthias Steinbacher, Ian Griffin, Jimmy Campbell, Max Burley, Marcus Warwick, Harika Vaka, Chizhou Fang, and Trevor William Clyne*

An attraction of the profilometry-based indentation plastometry (PIP) procedure is that, while it involves interrogation of volumes sufficiently large to ensure that bulk properties are obtained, it still allows stress–strain curves to be inferred for relatively small regions, such that local properties can be mapped where they are changing over short distances. It is employed here to obtain these characteristics as a function of depth in samples that have been case hardened by the diffusional penetration of carbon, to a depth of just over a mm. This has been done for a grade of steel that is commonly treated in this way. The thickness of the layer characterized by the PIP test is around 200 µm. In addition, curvature measurements on strip samples, after incremental removal of thin layers, have been used to evaluate the (compressive) residual stresses in near-surface regions. These range up to around 200 MPa. Such stresses have only a small effect on the PIP measurements. The carburization raises the peak yield stress from the base level of around 1000 MPa to about 1400 MPa, followed by considerable work hardening. The reliability of these PIP-derived stress–strain relationships has been confirmed by comparing experimental outcomes of Vickers hardness tests with FEM predictions based on their use.

1. Introduction

Profilometry-based inverse finite element method (FEM) for indentation plastometry (PIP) is a fairly novel mechanical testing methodology, involving FEM modeling of spherical indentation so as to converge on the best fit set of plasticity parameters (in a constitutive law), giving optimal agreement between experimental and predicted indent profiles. A recent review[1] covers the main issues involved in optimization of experimental and data processing procedures. There has also been detailed treatment of the effects of anisotropy,[2] residual stresses,[3] samples being exceptionally hard,[4] and use for measurement of property variations in and around fusion welds.[5]

The procedure offers many advantages over uniaxial testing, including reduced specimen preparation requirements and scope for mapping of properties on a relatively fine scale. The physical procedure is similar to hardness testing, but hardness numbers should be regarded as no better than semiquantitative guides to the plasticity of metals.[6] The fine scale mapping capability has already been applied to welds.[5] Another obvious application is provided by components in which particular regions—usually at free surfaces—have been deliberately hardened. This is often done to improve the resistance to wear or rolling contact fatigue, while leaving the interior relatively soft—commonly ensuring that it retains good toughness. Having quantitative information about the stress–strain relationships exhibited by material at different depths in such hardened layers is potentially of considerable value—for example, in predicting how the component will respond to service conditions, such as the application of bending moments or exposure to abrasive wear.

The spatial resolution obtainable via conventional uniaxial testing is clearly inadequate for this purpose. Nanoindentation apparently has excellent spatial mapping capabilities, but the

S. Ooi
Ovako Corporate R&D
Maxwell Centre
JJ Thompson Avenue, Cambridge CB3 0HE, UK

R. Reiff-Musgrove, J. Campbell, M. Burley, M. Warwick, H. Vaka, C. Fang, T. W. Clyne
Plastometrex Ltd.
204 Science Park, Milton Road, Cambridge CB4 0GZ, UK
E-mail: twc10@cam.ac.uk

M. Gaiser-Porter, T. W. Clyne
Department of Materials Science
University of Cambridge
27 Charles Babbage Road, Cambridge CB3 0FS, UK

M. Steinbacher
Leibniz-Institut für Werkstofforientierte Technologien – IWT
Badgasteiner Str. 3, 28359 Bremen, Germany

I. Griffin
Wallwork Heat Treatment Limited
Lord Street, Bury, Lancashire BL9 0RE, UK

volume being deformed is in most cases too small for its mechanical response to be representative of the bulk.[1] There have nevertheless been a few investigations[7–9] in which nano-indentation has been used to explore the material response as a function of depth into surface-hardened layers. However, this does not allow reliable stress–strain characteristics to be obtained for these hardened layers.

There has, however, been at least some previous work on exploring the mechanical response of case-hardened layers as a function of depth, using relatively large spherical indenters. In particular, the work of Moussa et al.[10] involved a 1 mm diameter cermet (WC–Co) ball, inverse FEM modeling, and use of load–displacement plots as target outcomes. The peak load was fixed at just under 1 kN, giving penetrations ranging from about 75 μm (into the original surface) to about 150 μm (after removal of the complete hardened layer, which was about 400 μm thick). They used a simple (2-parameter) strain hardening law, involving just the yield stress and a strain hardening exponent. One challenge with such investigations is that of validating the inferred stress–strain relationships (as a function of depth). In the Moussa study, this was approached by comparing an experimental load–displacement plot obtained by pushing a large cylindrical roller deep into the sample with the corresponding prediction from an FEM model in which indentation-derived stress–strain curves were used for six different depths. The agreement obtained was good, but this is a relatively insensitive test. The overall procedure employed is valid, although the combination of using load–displacement plots as target outcomes (rather than indent profiles) and employing a limited (2-parameter) constitutive law is likely to result in relatively low reliability. Furthermore, no account was taken of the possible presence of residual stresses in the case-hardened layer. In practice, such stresses may well be present, and are likely to be compressive in the case-hardened layer. Typical peak magnitudes in case-hardened steels of this type[11–13] are of the order of several hundred MPa. For example, Prime et al.[11] obtained a value of around 400 MPa in a 0.2 wt%C steel, near the free surface (where the C content had been raised to about 0.8 wt%). Such stresses can be beneficial because they will tend to inhibit plastic deformation and crack formation during service, but stress–strain relationships obtained without taking them into account could be somewhat unreliable.

A further relevant investigation is that of Astaraee et al.,[14] who examined the effect of shot peening a case-hardened layer. This work was partly a follow-up to that of Moussa et al. and they also used inverse FEM to infer the stress–strain relationship (captured in a 2-parameter constitutive law) at a given depth, with the target outcome again being measured load–displacement plots obtained during indentation with a very large (10 mm diameter) cermet sphere. (These conditions resemble those of the Brinell hardness test.) They also carried out the indentation experiments after progressive removal of surface layers. Part of the focus of their work was in fact on residual stresses, which are likely to be present in case-hardened layers and certainly tend to be induced by shot peening. They measured them directly via X-ray diffraction (XRD) and attempted to infer them from their indentation outcomes. They did confirm that there were compressive residual stresses in the carburized layer. Recent work[3] has indicated that the effect of residual stresses on PIP-inferred stress–strain curves is often relatively small, although it is not always negligible. Astaraee et al. also used hardness data in their analysis, involving the introduction of arbitrary curve-fitting parameters. Nevertheless, they were able to quantify at least some of the relevant factors involved.

The present work is focused on a first use of the PIP procedure, with a series of grinding operations, to obtain (true) stress–strain relationships, as a function of depth, within case-hardened layers. It also includes an investigation of the residual stresses in these layers, obtained by applying a layer removal and curvature measurement procedure to strip samples. Validation of the sets of stress–strain relationships within the case-hardened layers is tackled by comparing measured Vickers hardness numbers with the outcomes of FEM simulations of the test, obtained using the PIP-derived stress–strain relationships (as a function of depth).

2. Experimental Section

2.1. Material and Carburizing Treatment

The steel used in this work, designated 158Q, was developed by Ovako. Its composition (measured by Optical emission spectroscopy (OES) spectroscopy—see Section 2.2) is given in **Table 1**. It is an ingot cast case hardening steel, designed to minimize internal oxidation (during carburizing). Hot-rolled bars were machined into plates with dimensions of 140 × 100 × 3 mm. It was carburized, using the sequence shown in **Table 2**. The carbon potential values shown are those in thermodynamic equilibrium with the furnace atmosphere, which was a mixture of air and methane (in the presence of a Ni catalyst). The signal from a probe measuring the oxygen partial pressure was used to control the gas flow rate, to maintain the selected carbon potential. The carbon concentration profiles are reported in the next section.

After this treatment, the plates were cut into several strips, each with dimensions of 140 × 9 × 3 mm, using electrodischarge machining. This operation involved first removing the two sections (of thickness 2 mm) along the edges (into which

Table 1. Composition of the steel.

Composition [wt%]					
C	Si	Mn	Cr	Mo	Ni
0.19	0.08	0.25	0.37	0.68	2.28

Table 2. Treatment sequence and carbon potentials at different stages.

Stage	Carbon potential [wt%]
Heat to 930 °C and soak for 0.5 h	0.85
Gas carburize at 930 °C for 3 h	1.2
Diffuse at 930 °C for 1 h	0.85
Furnace cool to 820 °C	–
Soak at 820 °C for 1 h	0.85
Oil quench	–
Temper at 200 °C for 1 h	–

carburization took place laterally). The strips thus contained carburized layers on top and bottom surfaces (140 × 9 mm) only, with no penetration into the edge surfaces (140 × 3 mm). These strips were produced to measure the curvature after progressive removal of thin layers from one of the carburized surfaces, for purposes of inferring the distribution of residual stress within the removed layers—see Section 2.3.

2.2. Measurement of Carbon Profiles

Measurement of the carbon concentration profile created by the carburizing treatment was carried out on flat samples cut from the strips. These samples had a thickness of 3 mm, a length of 15 mm, and a width of 9 mm. They were mounted on a holder (using a two-component adhesive), to facilitate the multiple grinding steps used for carbon profile generation. This was performed using a spark-optical-emission-spectrometer S-OES ARL 3460 (Thermo Scientific). Emission analysis was calibrated using samples with carbon contents covering the range concerned (0.119, 0.225, 0.64, and 1.03 wt%C). Analysis was carried out on a series of surfaces, created by repeatedly grinding off thin layers. The outcome of these measurements is shown in **Figure 1**. Significant penetration of the diffusing carbon has occurred to a depth of around 1.5 mm (i.e., to the center of the strip).

2.3. Residual Stress Levels from Curvature Changes

2.3.1. Significance of Residual Stress for PIP Testing

The PIP procedure involves obtaining a stress–strain relationship for a near-surface region. This is done via iterative FEM modeling of the indentation process, changing the stress–strain relationship until optimum agreement is reached between measured and modeled indent profiles. A possible source of complication is the presence of (in-plane) residual stresses in the region being tested. This has already been investigated[3] in some detail, with the broad conclusion being that their effects are likely to be relatively small in most cases. However, they may in some cases
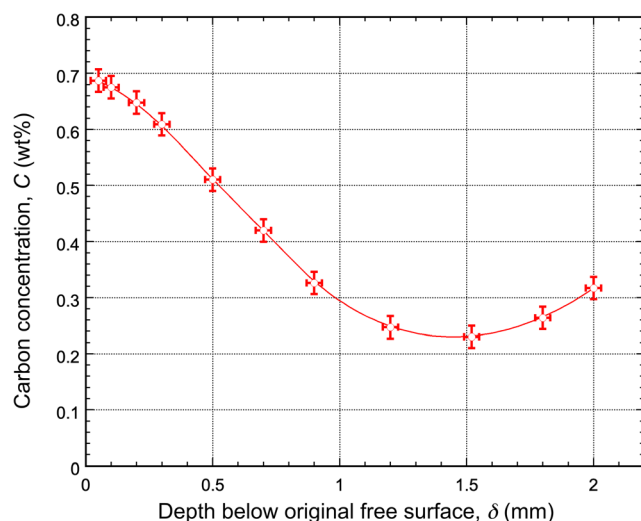
need to be incorporated into the FEM modeling, particularly in relatively hard materials, if fully reliable stress–strain relationships are to be obtained. There is certainly an expectation that they could be relatively high in case-hardened layers. An investigation was therefore carried out, aimed at quantifying the level and distribution of (equal biaxial) residual stresses in the regions to be indented.

A logical approach is to divide the case-hardened region into a discrete number of layers, within each of which it is assumed that there is a single residual stress level, and also a single stress–strain relationship. It is appropriate to set this layer thickness equal to the approximate depth interrogated during a PIP test—i.e., the region within which significant plastic deformation is being stimulated. Using a 1 mm radius ball, with a penetration ratio of around 10%, this depth is expected to be of the order of 200 μm. As, in the present case, the thickness of the case-hardened layer is of the order of 1 mm, this approach leads to a total of five depths being examined, before and after grinding away four layers of thickness 0.2 mm. Such a sequence of layer removal was therefore also used for assessment of residual stress levels, obtained by measuring the change in curvature of a strip sample each time (via profilometry).

2.3.2. Relationship between Curvature and Residual Stress

Extensive previous work has been carried out on relationships between stress levels in coatings and associated curvature. If the coating is much thinner than the substrate ($h \ll H$), then the Stoney equation[15] can reliably be employed. For the equal biaxial case, this can be written

$$\kappa = \frac{6h(1 - \nu_s)}{E_s H^2} \sigma_d \tag{1}$$

where k is the curvature, E_s and n_s are, respectively, the Young's modulus and Poisson ratio of the substrate, and σ_d is the stress in the coating ("deposit"). In such a case, a single stress level can be identified because only the coating is under stress and curvature formation has a negligible effect on this stress level.

The situation here, however, is somewhat different. Unlike the case of a deposited coating, it is not acceptable to assume that there is just a single stress level in it. It will be assumed that there are a discrete number of layers, with the stress level uniform in each one. Such cases can be analyzed, although the complexity level is higher than for the Stoney treatment.[16–19] Furthermore, relatively thin substrates must be used, to ensure that suitably large curvatures are generated. This leads to significant stress levels in both constituents, together with through-thickness gradients in them, caused by curvature adoption (**Figure 2**).

For such cases, the situation is best characterized in terms of a misfit strain ($\Delta\varepsilon$), rather than a stress level. The relationship between misfit strain and resultant curvature can be written[17]

$$\kappa = \frac{6E_s E_d (h + H) h H \Delta\varepsilon}{E_d^2 h^4 + 4E_d E_s h^3 H + 6E_d E_s h^2 H^2 + 4E_d E_s h H^3 + E_s^2 H^4} \tag{2}$$

where E_s and E_d are, respectively, the Young's moduli of substrate and coating; for an equal biaxial case such as here, these should have their "biaxial" values ($E' = E/(1-\nu)$).

Figure 1. Measured carbon concentration profile.

2201512 (3 of 10)
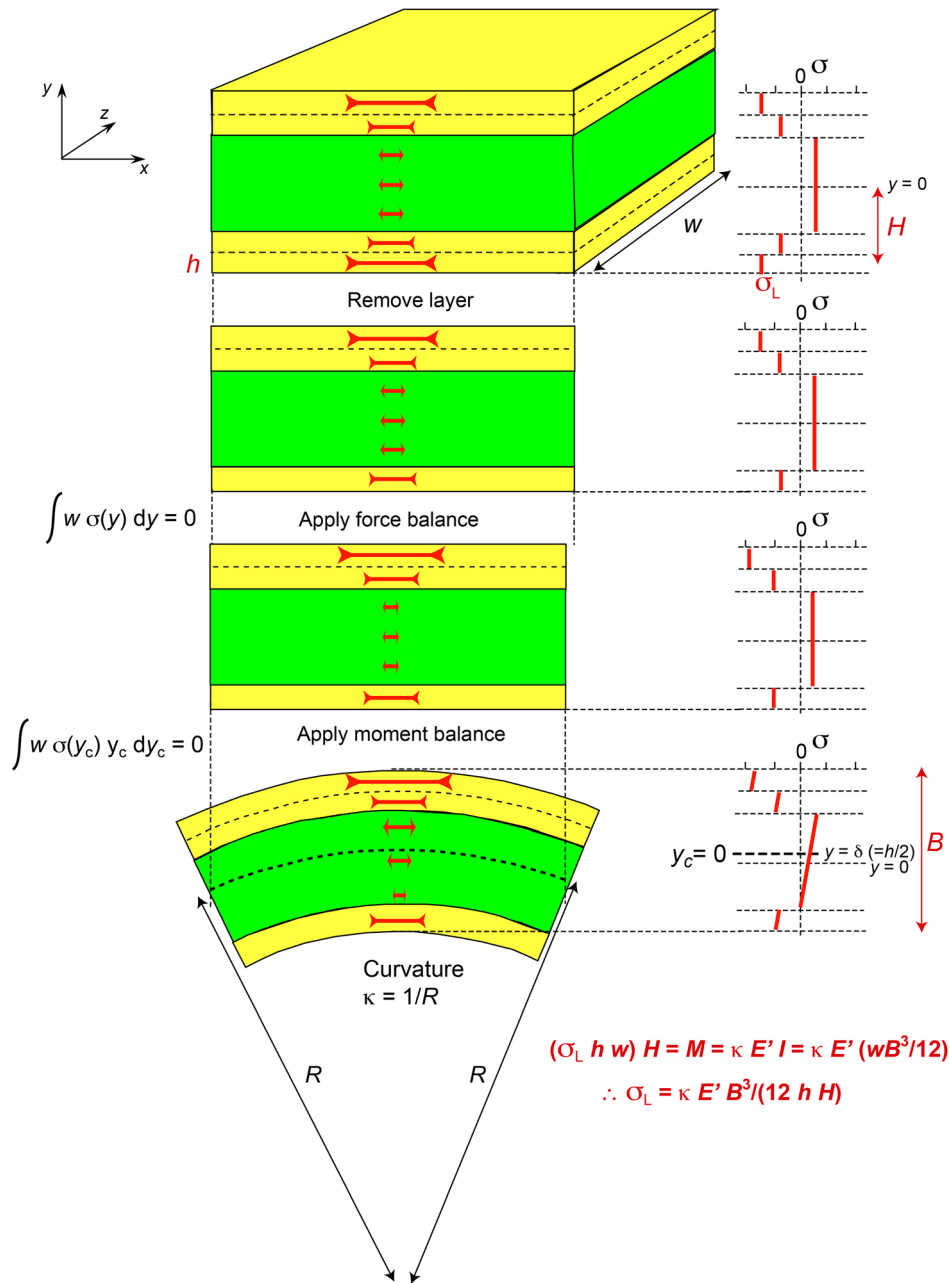
Figure 2. Schematic depiction of how curvature arises from the removal of a thin layer (containing residual stress) from the case-hardened region of a strip.
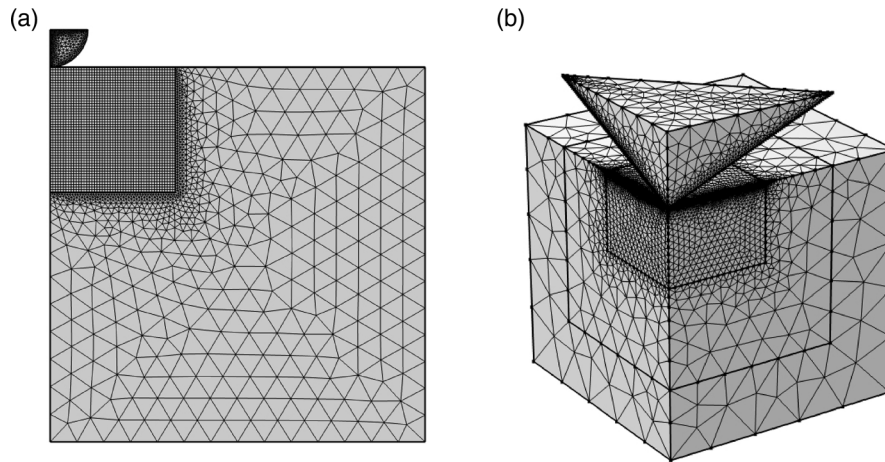
The current case is in fact simpler than the above one in some respects. The way that curvature arises is illustrated in **Figure 3**. One simplification is that the stiffness is the same everywhere (although the biaxial value must again be used). Moreover, if attention is focused on the stress level in the removed layer, then it is not necessary to take account of the stress gradients that are generated as curvature arises.

The bending moment, M, that is creating the curvature (or change in curvature), must have the same magnitude as that being produced by the stress in the layer before it was removed. It therefore follows that

$$(\sigma_{\mathrm{L}} h w) H = M = \kappa E' I = \kappa E' \left(\frac{w B^3}{12} \right) \tag{3}$$

where σ_{L} is the stress in the layer before it was removed, h is its thickness, H is the distance from the neutral axis to the center of the layer, w is the width of the strip, E' is the (biaxial) Young's modulus of the material, I is the second moment of area of the section of the strip, and B is the thickness of the strip (after layer removal). Equation (3) can be rearranged to give the (biaxial) stress in the layer in terms of the measured curvature (change) stimulated by its removal, k

**ADVANCED
SCIENCE NEWS**

www.advancedsciencenews.com

**ADVANCED
ENGINEERING
MATERIALS**

www.aem-journal.com

Figure 3. FEM meshes used for modeling of: a) spherical (PIP) indentation and b) Vickers hardness testing.

$$\sigma_{\mathrm{L}} = \frac{\kappa E' B^3}{12hH} \qquad (4)$$

For any given layer removal operation, the dimensions h, H, and B are known, as is the (biaxial) Young's modulus, so the residual stress in the removed layer can be obtained from the measured curvature (or, for removal of layers after the first one, from the change in curvature).

2.3.3. Machining Operation

Removal of thin layers from the strips was carried out by grinding with an abrasive wheel, the sample being held flat on the machining bed by a magnetic clamp. Grinding operations were carried out on the top surfaces only, removing 25 μm per pass. Thicknesses removed from the top surfaces were 200, 400, 600, and 800 μm. When released from the magnetic clamp, these samples adopted progressively increasing levels of curvature.

2.3.4. Curvature Measurement

The curvatures of the strips were measured using an optical interferometer (NetGAGE3D from Isra Vision) to obtain the height at a series of equally spaced points along the length of the sample, which was located on a horizontal surface with the convex side uppermost. The resolution of this technique is of the order of 5 μm. When converted to an average radius of curvature, which ranged from about 2 m up to around 10 m, the resolution is probably around 50 mm. These figures translate into the probable error on the derived curvature values being of the order of 0.02 m^{-1}. However, inelastic processes, such as induced plasticity or diffusional relaxation (promoted by temperature rises), could take place during grinding and are potential sources of error.

2.4. Indentation Plastometry (PIP Testing)

The PIP setup used is described in the literature.[5] The procedure involves creation of an indent by applying a known force,

followed by measurement of its (radially symmetric) profile. Iterative FEM simulation of the test is then carried out until the best fit set of plasticity parameter values has been obtained. The Voce (3-parameter) law has been found to be most effective in capturing the (true) stress–strain relationship exhibited by a wide range of metals—partly because it allows the true work hardening rate to approach zero at high strains, which is apparently quite common. Such issues are fully explored in a recent review article.[1] PIP testing was carried out before and after removal of several layers of thickness 200 μm, as described in Section 2.3.3. For tests on original outer surfaces, a thin (oxidized) layer (about 2 μm in thickness) was first removed by grinding. The balls used were Si$_3$N$_4$, with a radius, R, of 1 mm, and the penetration ratio, d/R, was around 10%. As noted in Section 2.3.1, the thickness of the layer thus being interrogated (undergoing significant plastic deformation) is not well defined, but is around 200 μm. Indent topographies were characterized with a stylus profilometer having a resolution of about 1 μm. The indents had a width of ≈1 mm.

In this context, there is some logic to characterizing the stress–strain relationship in layers with a thickness of the order of 200 μm because this was the thickness that was removed each time when assessing the distribution of residual stress, and also between each PIP test. The inferred relationship is taken to be an average over this thickness, even though it may be changing significantly over the range of depth concerned. For current illustrative purposes, this is considered appropriate. It may, however, be noted that improved resolution could be obtained by reducing the thickness removed each time and using a smaller ball. For example, balls of 0.5 mm radius are routinely available for PIP testing and, using a similar penetration ratio, the relationship would in that case be representative of a layer about 100 μm in thickness. This might be more appropriate for some purposes.

There is no prospect of being able to compare these stress–strain results with outcomes of conventional uniaxial (tensile or compressive) testing, so another validation procedure was needed. The approach adopted here was to compare Vickers hardness values obtained on a transverse surface at different

**ADVANCED
SCIENCE NEWS**

www.advancedsciencenews.com

**ADVANCED
ENGINEERING
MATERIALS**

www.aem-journal.com

depths with the outcomes of FEM simulation of the test, using the PIP-derived stress–strain relationship for the (range of) depth concerned.

2.5. Hardness Testing

A common way of characterizing the plasticity on a relatively fine scale, to explore properties in regions such as case-hardened layers, is to carry out hardness tests (on transverse sections). The major drawback to this is that hardness numbers are only semiquantitative indicators of the resistance to plastic deformation. However, it was undertaken here as a check on the reliability of the stress–strain relationships obtained via PIP testing (as these can be used to predict the plasticity response during any kind of loading, including that of a particular type of hardness test). Vickers hardness numbers were measured on transverse sections, using a Qness hardness machine.

2.6. FEM Modeling

For both the spherical indentation (PIP testing) and the Vickers hardness testing, FEM simulation was involved. For PIP, the simulation was carried out iteratively, whereas for the Vickers test it was just done once for each PIP-inferred set of Voce parameter values—that is, for each of the 200 μm-thick layers that were interrogated. Details of the PIP model have been described in previous publications, as mentioned above. Nevertheless, the meshes used in both types of model are shown in Figure 3. The elements used were 2D quadratic serendipity elements (4400 in total) for the PIP and 3D linear elements (129 657 in total) for the Vickers.
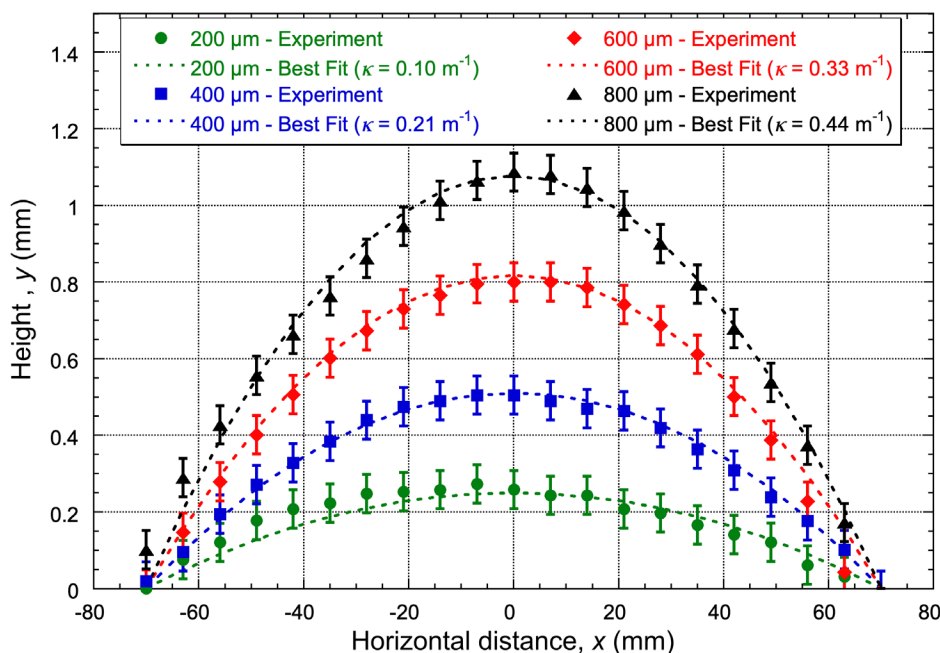
3. Residual Stresses

Comparisons are shown in **Figure 4** between measured height data, as a function of position along the length, and corresponding best fit uniform curvature plots. These were obtained using a simple least squares criterion. While there is some variation in curvature along the length, these values give a good overall representation of the sample shape. These curvature data are presented in **Table 3**, together with inferred residual stress values in the near-surface regions.

The residual stresses listed in Table 3 are all compressive—this is clear from the sense of the curvatures, which were all concave on the side from which the layers had been removed. This is as expected, with the carburizing causing an increase in volume. Realistically, the error on these values is relatively high, but they probably give a good indication of the order of magnitude of these stresses. The values are plotted in **Figure 5**. As expected, they drop off with depth. The values are broadly consistent with previously reported data, although a dependence on the carburization conditions (and the type of steel) is naturally expected.

Table 3. Curvature data and inferred residual stresses. The σ_L values were obtained from the (change in) curvature, using Equation (4). In all cases, the biaxial Young's modulus, E', was taken to be 286 GPa.

Total thickness removed [μm]	Average measured curvature, k [m^{-1}]	Δk [m^{-1}]	B [mm]	H [mm]	h [μm]	σ_L [MPa]
200	0.10	0.10	2.8	1.4	200	190
400	0.21	0.11	2.6	1.3	200	180
600	0.33	0.12	2.4	1.2	200	165
800	0.44	0.11	2.2	1.1	200	125

Figure 4. Comparison, for each layer thickness removed, between experimental height–distance measurements and corresponding best fit uniform curvature plots.
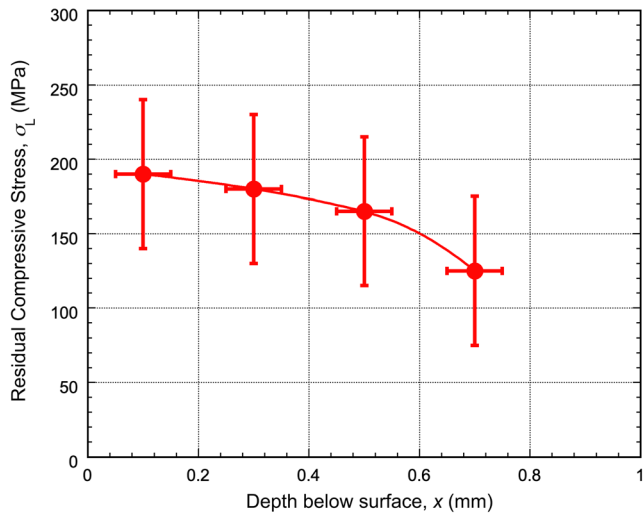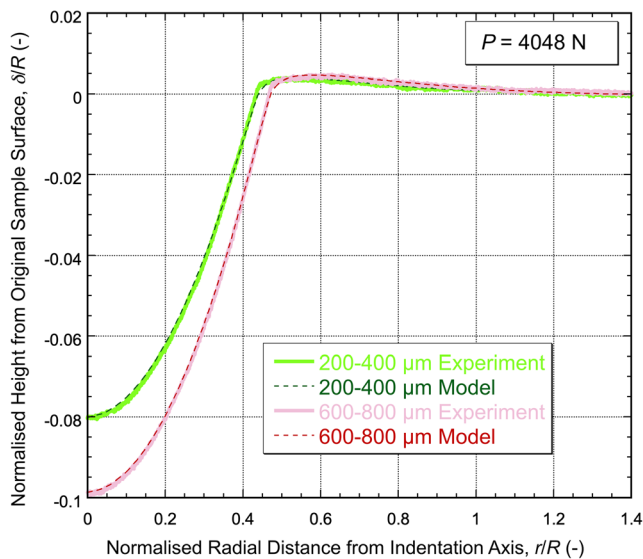
Figure 5. Curvature-derived residual stress levels within the carburized layer.

4. PIP Test Outcomes

4.1. Indent Profiles

A representative pair of measured indent profiles is shown in **Figure 6**, with the corresponding best fit modeled profiles included for comparison. The changes in the profiles confirm that the material gets softer with increasing depth below the original free surface (as expected). The Voce parameter sets corresponding to the best fit profile give the true stress–strain curve for the surface concerned. As the depth to which deformation is taking place is of the order of 200 μm, this stress–strain relationship can be taken to be representative of a layer with approximately this thickness.

4.2. Inferred Stress–Strain Curves

The outcomes of these PIP tests, in the form of sets of Voce parameter values, are presented in **Table 4**. These sets of values define true stress–true plastic strain curves exhibited by material, as a function of depth (averaged over 200 μm increments of thickness). These curves represent a fundamental characterization of the plasticity response of the material. However, such information is commonly presented in the form of a nominal stress–nominal strain relationship, as would be obtained in a tensile test. Conversion between the two types of curve is carried out using the following well-known equations (based on conservation of volume during plastic deformation)
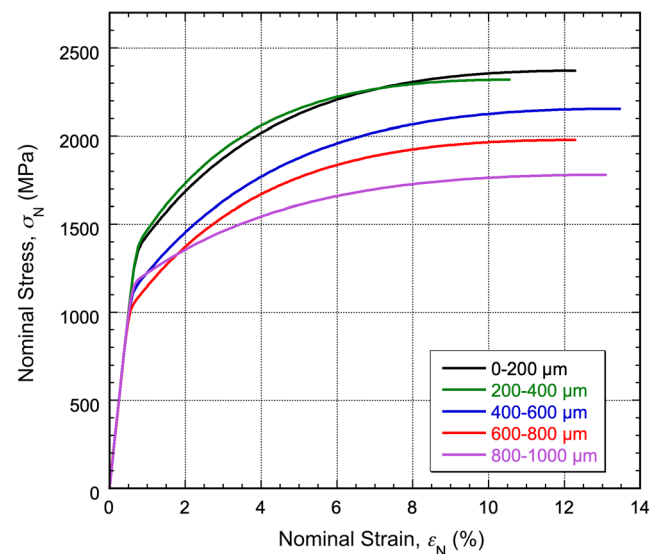
$$\sigma_T = \sigma_N(1 + \varepsilon_N) \tag{5}$$

$$\varepsilon_T = \ln(1 + \varepsilon_N) \tag{6}$$

where the subscripts T and N refer to true and nominal values. It should be noted, however, that these equations only apply while

**Table 4.** Sets of Voce parameter values obtained by PIP testing.

Thickness range [μm]	Yield stress σ_Y [MPa]	Saturation stress σ_s [MPa]	Characteristic strain ε_0 [%]
0–200	1340	2767	4.4
200–400	1365	2643	3.6
400–600	1104	2554	4.9
600–800	1013	2307	4.3
800–1000	1156	2114	5.5

Figure 6. Measured and (best fit) modeled indent profiles on two surfaces at different depths below the original free surface. The radius of the indentation sphere was 1 mm in all cases.

Figure 7. PIP-inferred tensile (nominal) stress–strain curves for layers at different locations below the original free surface.

**ADVANCED
SCIENCE NEWS**

www.advancedsciencenews.com

**ADVANCED
ENGINEERING
MATERIALS**

www.aem-journal.com

the stress and strain fields are uniform—so they are not valid after the onset of necking (which occurs at the peak of a nominal plot).

The nominal curves (for tensile loading) are shown in **Figure 7**. The behavior is broadly as expected, with the yield stress rising from around 1000 MPa in the interior to ≈1400 MPa near the free surface. Appreciable work hardening is exhibited in all cases.
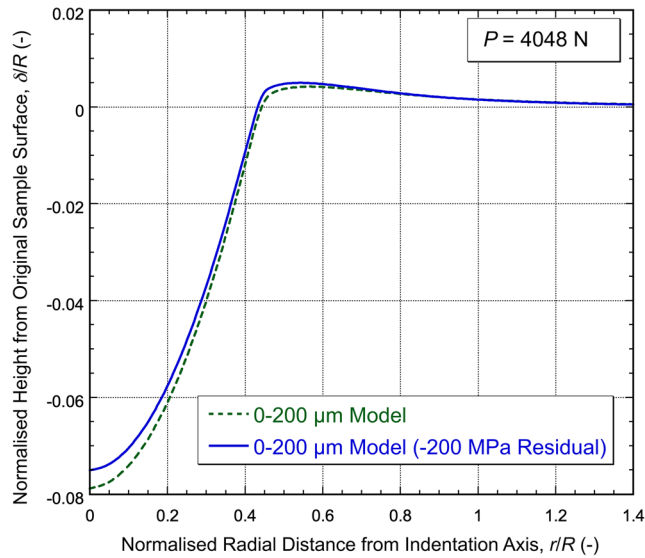

Figure 8. Modeled indent profiles for penetration of a 1 mm radius ball into the top layer, with and without a compressive residual stress of 200 MPa.

4.3. Effect of Residual Stresses

As outlined above, residual stresses can affect the way that indentation takes place, and hence influence the residual indent profile. However, one outcome of a detailed investigation into this issue[3] was that the effect tends in most cases to be relatively small, particularly for compressive residual stresses. Such stresses tend to retard initial yielding during PIP testing (whereas tensile residual stresses accelerate it). However, after considerable penetration has taken place, the stress field around the indenter is often little different from that in the absence of residual stress. In the current case, in which the residual stresses in the near-surface region are compressive and relatively low, the effect is negligible. This can be seen from **Figure 8**, which shows predicted indent profiles for the top layer (first set of Voce parameter values in Table 4), with and without the presence of a compressive residual stress of 200 MPa. The effect of the residual stress is small—almost within the margin of experimental error expected in measuring the profile. As this case is the most severe (highest residual stress), the error involved in neglecting residual stress in all cases is expected to be very small.

5. Validation via Hardness Testing

The FEM modeling of the Vickers test, carried out using the Voce parameter sets in Table 4, leads to 3D indent profiles. In the test itself, the hardness numbers are obtained by measuring the average of the two diameters (in projection). For a transversely isotropic material, these two should be the same. When obtaining values from modeling of the test, a decision must be made about how this diameter would be perceived when viewed in the optical
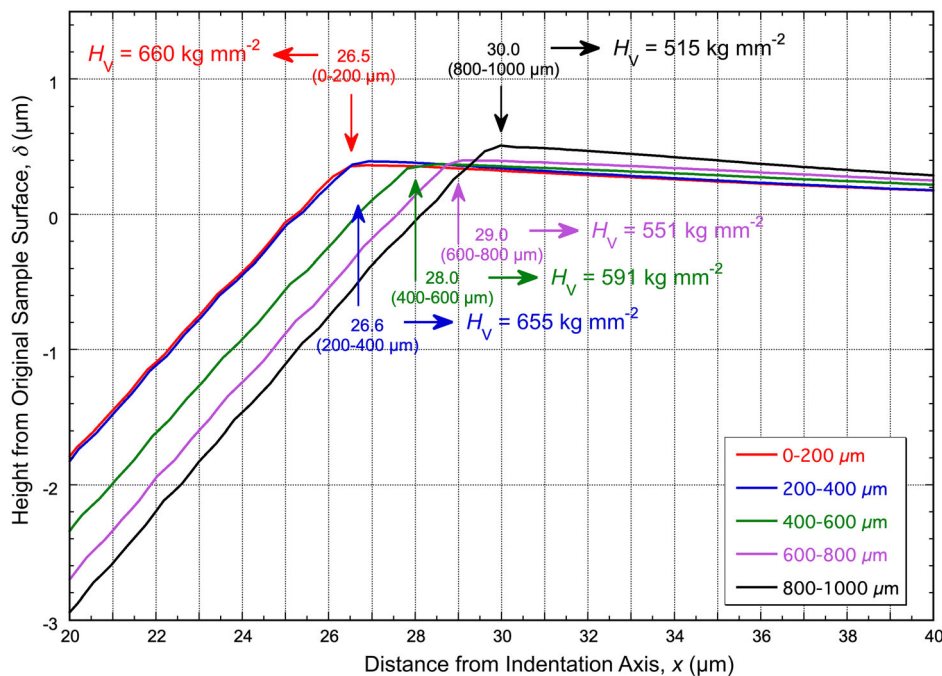
Figure 9. FEM-predicted Vickers indent profiles (along the diagonals) for the Voce sets shown in Table 4, with an indication of the (semi-) diameter values that would probably be obtained when viewed in the optical microscope, and corresponding H_V values.
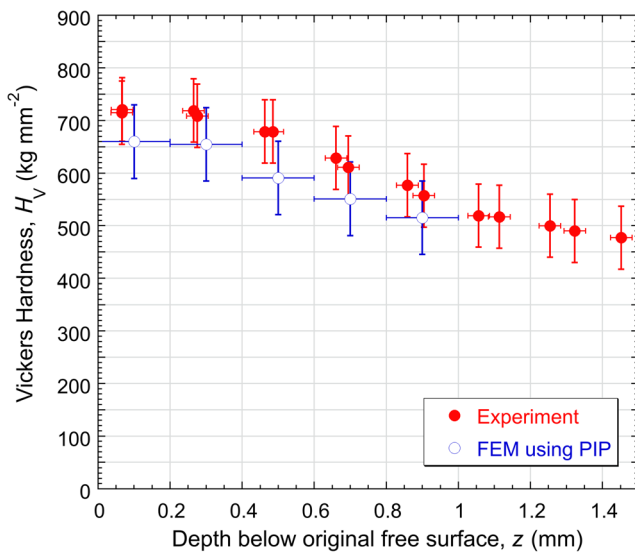
Figure 10. Comparison between directly measured Vickers hardness numbers ($P = 1$ kg), as a function of depth, and corresponding values obtained by FEM modeling of the test, using PIP-derived stress–strain relationships.

microscope. The modeled profiles are shown in **Figure 9**, with these perceived (semi-) diameters taken to be the distance from the indentation axis to the highest point of the pile-up created by the indentation. The Vickers hardness number is then obtained from the standard equation

$$H_V = 1.854 \frac{F}{d^2} \tag{7}$$

where F is the applied force and d is the diagonal length. This corresponds to the force over the contact area, based on a simple geometrical construction (neglecting any effects of pile-up, sink-in, or spring-back). Hardness numbers have little or no intrinsic significance, but can be used in this instance to explore the reliability of the inferred stress–strain relationships.

A comparison is shown in **Figure 10** between experimental Vickers hardness numbers, as a function of depth below the free surface, and corresponding values obtained via the FEM simulation. The agreement is good, although it should be recognized that both experimental measurements and inferred values are subject to considerable error, particularly for vary hard material of this type. In this regime, an error of a micron or so in measured diameter changes the H_V value by about 10%. It should also be noted that, in view of the fairly sharp gradient in hardness, PIP testing with an interrogated depth of around 200 μm will tend to give stress–strain curves that are slightly below the actual ones. This may account for the FEM-derived values being slightly below the directly measured ones. Nevertheless, the broad consistency is clear.

6. Conclusions

The following conclusions can be drawn from this work, which is focused on use of the PIP technique to obtain stress–strain relationships as a function of depth within a case-hardened layers

(≈ 1 mm thick) for a particular steel: 1) The carburizing creates (compressive) residual stress in the near-surface regions. This has been investigated by measuring the curvatures induced in strip samples (carburized on both sides) as thin layers are repeatedly ground away on one side. These (equal biaxial) stresses range up to about 200 MPa. 2) PIP testing has been carried out on free surfaces, with and without prior grinding away of thin layers. In this way, (true) stress–strain curves were obtained that are representative of those in a series of near-surface layers, each about 200 μm in thickness. While the yield stress of the steel before carburizing was around 1000 MPa, it ranged up to about 1400 MPa at the as-carburized surface. The PIP outcomes also indicate relatively high rates of work hardening in all cases. 3) Validation of these sets of stress–strain curves has been approached by comparing Vickers hardness numbers obtained on transverse surfaces at a series of depths below the original free surface with predicted numbers obtained by FEM simulation of the Vickers test, carried out using stress–strain relationships derived from PIP testing of free surfaces after grinding away a series of thin layers. Good agreement is observed across the complete range of depth.

Conflict of Interest

The authors declare no conflict of interest.

Data Availability Statement

The data that support the findings of this study are available from the corresponding author upon reasonable request.

[1] T. W. Clyne, J. E. Campbell, M. Burley, J. Dean, *Adv. Eng. Mater.* **2021**, *23*, 21004037.

[2] Y. T. Tang, J. E. Campbell, M. Burley, J. Dean, R. C. Reed, T. W. Clyne, *Materialia* **2021**, *15*, 101017.

[3] M. Burley, J. E. Campbell, R. Reiff-Musgrove, J. Dean, T. W. Clyne, *Adv. Eng. Mater.* **2021**, *23*, 2001478.

[4] J. E. Campbell, M. Gaiser-Porter, W. Gu, S. Ooi, M. Burley, J. Dean, T. W. Clyne, *Adv. Eng. Mater.* **2022**, *24*, 2101398.

[5] W. Gu, J. E. Campbell, Y. T. Tang, H. Safaie, R. Johnston, Y. Gu, C. Pleydell-Pearce, M. Burley, J. Dean, T. W. Clyne, *Adv. Eng. Mater.* **2022**, *24*, 2101645.

[6] T. W. Clyne, J. E. Campbell, *Testing of the Plastic Deformation of Metals*, Cambridge University Press, Cambridge, UK **2021**, https://doi.org/10.1017/9781108943369.

[7] H. Elghazal, G. Lormand, A. Hamel, D. Girodin, A. Vincent, *Mat. Sci. Eng. A* **2001**, *303*, 110.

[8] D. Terentyev, A. Bakaeva, T. Pardoen, A. Favache, E. E. Zhurkin, *J. Nucl. Mater.* **2016**, *476*, 1.

[9] S. I. Chugunova, Y. V. Milman, A. I. Lukyanov, I. V. Goncharova, *Powder Metall. Met. Ceram.* **2022**, *60*, 331.

[10] C. Moussa, O. Bartier, G. Mauvoisin, X. Hernot, J. M. Collin, G. Delattre, *Surf. Coat. Technol.* **2014**, *258*, 782.

[11] M. B. Prime, V. C. Prantil, P. Rangaswamy, F. P. Garcia, in *ECRS 5: Proc. of the Fifth European Conf. on Residual Stresses* (Eds: A. J. Bottger, R. Delhez, E. J. Mittemeijer), Publisher is Materials Research Forum **2000**, p. 223, https://doi.org/10.4028/www.scientific.net/MSF.347-349.223.

[12] T. Krug, K. H. Lang, T. Fett, D. Lohe, *Mat. Sci. Eng. A* **2007**, *468*, 158.

[13] Y. Sakaida, S. Yamashita, M. Manzanka, in *8th European Conf. on Residual Stresses (ECRS 8)*, Riva del Garda, Italy, June 26–28 **2010**, https://doi.org/10.4028/www.scientific.net/MSF.681.346.

[14] A. H. Astaraee, S. Bagherifard, A. Bradanini, P. Duo, S. Henze, B. Taylor, M. Guagliano, *Surf. Coat. Technol.* **2020**, *398*, 126084.

[15] G. C. A. M. Janssen, M. M. Abdalla, F. v. Keulen, B. R. Pujada, B. v. Venrooy, *Thin Solid Films* **2009**, *517*, 1858.

[16] L. B. Freund, J. A. Floro, E. Chason, *Appl. Phys. Lett.* **1987**, *74*, 1987.

[17] T. W. Clyne, *Key Eng. Mater.* **1996**, *116/7*, 307.

[18] Y. C. Tsui, T. W. Clyne, *Thin Solid Films* **1997**, *306*, 23.

[19] J. Dean, T. Gu, T. W. Clyne, *Surf. Coat. Technol.* **2015**, *269*, 47.

2201512 (10 of 10)